Inorg. Chem. **2008**, *47*, 6873−6879

Syntheses, Structures, Physical Properties, and Electronic Properties of Some $AMUQ_3$ Compounds (A = Alkali Metal, M = Cu or Ag, Q = S or Se)

Jiyong Yao,[†] Daniel M. Wells,[†] George H. Chan,[†] Hui-Yi Zeng,[†] Donald E. Ellis,[†,‡] Richard P. Van Duyne,[†] and James A. Ibers*[,†]

Department of Chemistry, Northwestern University, Evanston, Illinois 60208-3113, and Department of Physics and Astronomy, Northwestern University, Evanston, Illinois 60208-3112

Received March 12, 2008; Accepted May 6, 2008

The seven new isostructural quaternary uranium chalcogenides $KCuUS_3$, $RbCuUS_3$, $RbAgUS_3$, $CsCuUS_3$, $CsAgUS_3$, $RbAgUSe_3$, and $CsAgUSe_3$ were prepared from solid-state reactions. These isostructural materials crystallize in the layered $KZrCuS_3$ structure type in the orthorhombic space group *Cmcm*. The structure is composed of UQ_6 octahedra and MQ_4 tetrahedra that share edges to form $^2_\infty[UMQ_3^-]$ layers. These layers stack perpendicular to [010] and are separated by layers of face- and edge-sharing AQ_8 bicapped trigonal prisms. There are no Q−Q bonds in the structure, so the formal oxidation states of A/U/M/Q may be assigned as 1+/4+/1+/2−, respectively. $CsCuUS_3$ shows semiconducting behavior with thermal activation energy $E_a = 0.14$ eV and $\sigma_{298} = 0.3$ S/cm. From single-crystal absorption measurements in the near IR range, the optical band gaps of these compounds are smaller than 0.73 eV. The more diffuse 5f electrons play a much more dominant role in the optical properties of the $AMUQ_3$ compounds than do the 4f electrons in the $AMLnQ_3$ compounds (Ln = rare earth). Periodic DFT spin band-structure calculations on $CsCuUS_3$ and $CsAgUS_3$ establish two energetically similar antiferromagnetic spin structures and show magnetic interactions within and between the layers of the structure. Density-of-states analysis shows M−Q orbital overlap in the valence band and U−Q orbital overlap in the conduction band.

Introduction

Recently, the 3d/4f solid-state $AMLnQ_3$ chalcogenides (A = alkali metal; M = Zn, Cd, Hg, Mn, or Co; Ln = Y or rare-earth element; Q = S, Se, Te) have been investigated.[1–6] Although all of these compounds adopt the $KZrCuS_3$ structure type,[7] they show different magnetic and optical properties depending on the combination of elements involved. Far fewer 3d/5f solid-state compounds are known than 3d/4f solid-state compounds. Actinide (5f) compounds often exhibit interesting magnetic and electronic properties different from those of the corresponding rare-earth (4f) compounds owing to the more diffuse nature of the 5f orbitals compared to the 4f orbitals. Among the reported quaternary 3d/5f chalcogenides, those of U possessing the $KZrCuS_3$ structure type are $KCuUSe_3$,[8] $CsCuUSe_3$,[1] and $CsCuUTe_3$.[9] Note that there are no reports of $AMUQ_3$ compounds for Q = S or M ≠ Cu. As shown for the $AMLnQ_3$ lanthanides, different magnetic and optical properties result from different combinations of elements. Thus, it is important to synthesize additional 5f compounds, especially sulfides, to obtain a better understanding of structure−property relationships.

* To whom correspondence should be addressed. Phone: +1 847 491 5449. Fax: +1 847 491 2976. E-mail: ibers@chem.northwestern.edu.
[†] Department of Chemistry.
[‡] Department of Physics and Astronomy.

(1) Huang, F. Q.; Mitchell, K.; Ibers, J. A. *Inorg. Chem.* **2001**, *40*, 5123–5126.
(2) Mitchell, K.; Haynes, C. L.; McFarland, A. D.; Van Duyne, R. P.; Ibers, J. A. *Inorg. Chem.* **2002**, *41*, 1199–1204.
(3) Mitchell, K.; Huang, F. Q.; McFarland, A. D.; Haynes, C. L.; Somers, R. C.; Van Duyne, R. P.; Ibers, J. A. *Inorg. Chem.* **2003**, *42*, 4109–4116.
(4) Mitchell, K.; Huang, F. Q.; Caspi, E. N.; McFarland, A. D.; Haynes, C. L.; Somers, R. C.; Jorgensen, J. D.; Van Duyne, R. P.; Ibers, J. A. *Inorg. Chem.* **2004**, *43*, 1082–1089.
(5) Yao, J.; Deng, B.; Sherry, L. J.; McFarland, A. D.; Ellis, D. E.; Van Duyne, R. P.; Ibers, J. A. *Inorg. Chem.* **2004**, *43*, 7735–7740.
(6) Chan, G. H.; Sherry, L. J.; Van Duyne, R. P.; Ibers, J. A. *Z. Anorg. Allg. Chem.* **2007**, *633*, 1343–1348.
(7) Mansuetto, M. F.; Keane, P. M.; Ibers, J. A. *J. Solid State Chem.* **1992**, *101*, 257–264.
(8) Sutorik, A. C.; Albritton-Thomas, J.; Hogan, T.; Kannewurf, C. R.; Kanatzidis, M. G. *Chem. Mater.* **1996**, *8*, 751–761.
(9) Cody, J. A.; Ibers, J. A. *Inorg. Chem.* **1995**, *34*, 3165–3172.

10.1021/ic800424t CCC: $40.75
Published on Web 07/02/2008

Table 1. Crystal Data and Structure Refinements for Seven $AMUQ_3$ Compounds[a]

	$KCuUS_3$	$RbCuUS_3$	$RbAgUS_3$	$CsCuUS_3$	$CsAgUS_3$	$RbAgUSe_3$	$CsAgUSe_3$
fw	436.85	483.22	527.55	530.66	574.99	668.25	715.69
a (Å)	3.9711(6)	3.9885(4)	4.0819(7)	3.9997(7)	4.0982(10)	4.2060(5)	4.2190(4)
b (Å)	13.894(2)	14.3991(16)	14.473(2)	15.172(3)	15.168(4)	14.9188(17)	15.6610(16)
c (Å)	10.2903(15)	10.2961(12)	10.4646(17)	10.3257(18)	10.505(3)	10.8140(12)	10.8440(11)
V (Å^3)	567.75(15)	591.31(11)	618.20(18)	626.62(19)	653.0(3)	678.56(13)	716.50(12)
T (K)	293(2)	153(2)	153(2)	153(2)	153(2)	153(2)	153(2)
ρ_{calcd} (g/cm^3)	5.111	5.428	5.668	5.625	5.849	6.541	6.635
μ (cm^{-1})	339.06	400.30	380.17	357.83	340.80	498.05	454.26
$R(F)^b$	0.0198	0.0250	0.0408	0.0196	0.0195	0.0260	0.0241
$R_w(F_o^2)^c$	0.0560	0.0635	0.1215	0.0447	0.0477	0.0662	0.0559
z	0.02	0.03	0.07	0.02	0.03	0.04	0.03

[a] For all structures $Z = 4$, space group = *Cmcm*, and $\lambda = 0.71073$ Å. [b] $R(F) = \sum||F_o| - |F_c||/\sum|F_o|$ for $F_o^2 > 2\sigma(F_o^2)$. [c] $R_w(F_o^2) = \{\sum [w(F_o^2 - F_c^2)^2]/\sum wF_o^4\}^{1/2}$ for all data. $w^{-1} = \sigma^2(F_o^2) + (z \times P)^2$, where $P = (F_o^2 + 2 \times F_c^2)/3$ for $F_o^2 > 0$; $w^{-1} = \sigma^2(F_o^2)$ for $F_o^2 \leq 0$.

Table 2. Selected Interatomic Distances (Angstroms) and Angles (Degrees)

	$KCuUS_3$	$RbCuUS_3$	$RbAgUS_3$	$CsCuUS_3$	$CsAgUS_3$	$RbAgUSe_3$	$CsAgUSe_3$
A−Q1 × 2	3.190(3)	3.310(2)	3.314(4)	3.471(2)	3.476(2)	3.416(1)	3.576(1)
A−Q2 × 4	3.334(2)	3.4252(2)	3.587(3)	3.567(1)	3.554(2)	3.6166(9)	3.7453(7)
A−Q2 × 2	3.585(2)	3.626(2)	3.468(4)	3.702(1)	3.706(2)	3.614(1)	3.6917(8)
U−Q1 × 2	2.7165(9)	2.7085(8)	2.759(2)	2.7064(7)	2.759(1)	2.8750(5)	2.8715(4)
U−Q2 × 4	2.714(1)	2.718(1)	2.747(2)	2.7232(9)	2.750(1)	2.8693(6)	2.8723(5)
M−Q1 × 2	2.405(2)	2.407(1)	2.548(3)	2.413(1)	2.552(2)	2.6429(9)	2.6470(9)
M−Q2 × 2	2.321(2)	2.324(2)	2.485(4)	2.327(2)	2.490(2)	2.5927(9)	2.5972(8)
Q1−M−Q1	111.3(1)	111.9(1)	106.45(18)	111.95(8)	106.83(9)	105.45(5)	105.68(5)
Q1−M−Q2	107.81(3)	107.37(3)	105.97(5)	106.95(2)	105.48(3)	107.36(1)	106.88(1)
Q2−M−Q2	114.4(1)	115.6(1)	125.3(2)	117.20(8)	126.79(9)	120.96(5)	122.54(4)
Q1−U−Q2	90.62(5)	90.73(5)	93.8(1)	90.88(4)	93.49(5)	94.51(2)	94.34(2)
Q2−U−Q2	85.95(6)	85.60(5)	84.0(1)	85.49(4)	83.68(6)	85.73(2)	85.48(2)
Q1−U−Q1	180	180	180	180	180	180	180

Here, we extend this chemistry to report the synthesis, structure, magnetic, conductivity, optical, and electronic properties of the isostructural $AMUQ_3$ compounds $KCuUS_3$, $RbCuUS_3$, $RbAgUS_3$, $CsCuUS_3$, $CsAgUS_3$, $RbAgUSe_3$, and $CsAgUSe_3$.

Experimental Section

Syntheses. The following reagents were used as obtained: Rb (Aldrich, 98+%), Cs (Aldrich, 99.5%), Cu (Aldrich, 99.999%), Ag (Aldrich, 99.99+%), U (depleted, ORNL), S (Alfa Aesar, 99.99%), Se (Cerac, 99.99%). The compounds A_2Q_3 (A = Rb, Cs; Q = S, Se), the reactive fluxes[10] employed in the syntheses, were prepared by stoichiometric reactions of the elements in liquid NH_3. For the syntheses of $RbCuUS_3$, $RbAgUS_3$, $CsCuUS_3$, $CsAgUS_3$, $RbAgUSe_3$, and $CsAgUSe_3$, reaction mixtures of 0.12 mmol A_2Q_3, 0.05 mmol M (M = Cu or Ag), 0.10 mmol U, and 0.54 mmol Q were loaded into fused-silica tubes under an argon atmosphere in a glovebox. These tubes were sealed under a 10^{-4} Torr atmosphere and then placed in a computer-controlled furnace. The samples were heated to 373 K in 15 h, kept at 373 K for 20 h, then heated to 873 K in 6 h, kept at 873 K for 4 days, slowly cooled at 4 K/h to 523 K, and then the furnace was turned off. The reaction mixtures were washed free of flux with *N*,*N*-dimethylformamide and then dried with acetone. The products consisted of black needles of the $AMUQ_3$ compounds. The yields ranged from 10−40% based on M. Analysis of these compounds with an EDX-equipped Hitachi S-3500 SEM showed the presence of A, M, U, and Q. The compounds are stable in air for several weeks.

The compound $KCuUS_3$ was obtained in an exploration of another system. Initially, 0.40 mmol US_2 and 0.10 mmol Cu_2S were ground and loaded into a fused-silica tube in a glovebox. The tube was sealed under a 10^{-4} Torr atmosphere and heated at 1273 K for 10 days. The contents of the tube were then mixed with 0.10 mmol CaS and 2.3 mmol KBr, ground, and sealed in another fused-silica tube. This tube was heated to 1123 K in 60 h, kept at 1123 K for 240 h, and then slowly cooled at 3 K/h to 853 K, and then the furnace was turned off. The mixture was washed with water and then dried with acetone to afford black needles of $KCuUS_3$ in about 10% yield.

Structure Determinations. Single-crystal X-ray diffraction data were collected with the use of graphite-monochromatized Mo Kα radiation ($\lambda = 0.71073$ Å) on a Bruker Smart-1000 CCD diffractometer.[11] The crystal-to-detector distance was 5.023 cm. Crystal decay was monitored by recollecting 50 initial frames at the end of data collection. Data were collected by a scan of 0.3° in ω in groups of 606 frames at φ settings of 0, 90, 180, and 270° for all the compounds except $CsCuUS_3$ for which groups of 606 frames at φ settings of 0, 120, and 240° were collected. The exposure times varied from 10 to 25 s/frame. The collection of the intensity data was carried out with the program *SMART*.[11] Cell refinement and data reduction were carried out with the use of the program *SAINT*,[11] and face-indexed absorption corrections were performed numerically with the use of the program *XPREP*.[12] Then the program *SADABS*[11] was employed to make incident beam and decay corrections.

The structures were solved with the direct-methods program *SHELXS* and refined with the least-squares program *SHELXL*.[12] Each final refinement included anisotropic displacement parameters. A secondary extinction correction was necessary for all the compounds except $CsAgUS_3$. The program *STRUCTURE TIDY*[13] was then employed to standardize the atomic coordinates in each structure.

(10) Sunshine, S. A.; Kang, D.; Ibers, J. A. *J. Am. Chem. Soc.* **1987**, *109*, 6202–6204.
(11) *SMART, Version 5.054, Data Collection and SAINT-Plus Version 6.45a Data Processing Software for the SMART System*; Bruker Analytical X-Ray Instruments, Inc.: Madison, WI, USA, 2003.
(12) Sheldrick, G. M. *Acta Crystallogr., Sect. A* **2008**, *64*, 112–122.
(13) Gelato, L. M.; Parthé, E. *J. Appl. Crystallogr.* **1987**, *20*, 139–143.

Additional experimental details are given in Table 1 and in the Supporting Information. Selected metrical data are given in Table 2.

Single-Crystal Optical Measurement. Absorption measurements over the range of 900 nm (1.38 eV) to 1700 nm (0.73 eV) at 293 K were performed on single crystals of AUMS$_3$ (A = Rb. Cs; M = Cu, Ag) by methods described earlier.[4,6] Unpolarized light was used because the polarization filter does not function in the near-infrared region. The absorbance spectra of light perpendicular to both the (010) and (001) crystal faces were collected.

Electronic Conductivity Measurement. The electrical resistivity of a single crystal of CsCuUS$_3$ was measured along [100] between 2.0 and 400 K by standard four-probe ac methods with the use of a Quantum Design PPMS instrument. A crystal, 902 μm in length, was mounted with four leads constructed of 15 μm diameter copper wire and 8 μm diameter graphite fibers, and attached with Dow 4929N silver paint.

Theoretical Methodology. Periodic spin band-structure calculations were performed on the structures of CsCuUS$_3$ and CsAgUS$_3$ with the use of the first-principles DFT program VASP (Vienna ab initio Simulation Package) in which pseudopotentials with a plane-wave basis were applied.[14–17] The exchange-correlation potential was chosen as the generalized gradient approximation (GGA) in a projector augmented wave (PAW) method developed by Kresse and Joubert.[18] Automatically generated Monkhorst−Pack grids were used to carry out Brillouin zone integrations.[19] 6 × 6 × 6 *k*-point meshes were chosen for relaxations and total energy calculations; these were increased to 8 × 8 × 8 for establishing convergence and again to 9 × 9 × 9 to confirm magnetic stability; *k*-point meshes were increased to 11 × 11 × 11 for calculations of densities of states (DOS). Ionic relaxations were conducted in the fixed 153 K unit cells (Table 1) and convergence was established when forces on each ion relaxed below 0.02 eV/Å.

The electrons described as core in the PAW potentials are those comprising [Xe] for Cs leaving 9 valence electrons per atom as $5s^2 5p^6 6s^1$; [Ar] for Cu and [Kr] for Ag leaving 11 valence electrons per atom as $d^{10}s^1$; [Xe]$5d^{10}4f^{14}$ for U leaving 14 valence electrons per atom as $5f^3 6s^2 6p^6 6d^1 7s^2$; and [Ne] for S leaving 6 valence electrons per atom as $3s^2 3p^4$. Calculations were conducted on a 24 atom crystallographic unit cell in the orthorhombic space group *Cmcm*; atomic positions were relaxed but unit cell constants were not varied. For consideration of possible spin structures, the magnetic unit cell was taken as the crystallographic unit cell. Owing to the unknown nature of the magnetic moments of the M or U atoms, initial electronic spin relaxations of CsCuUS$_3$ and CsAgUS$_3$ were conducted in which a moment on either one U or one M site was allowed to propagate throughout the structure. Calculations were reinitialized with the determined spin structures and carried to convergence. Oxidation states were investigated by means of electron density surfaces determined by volume integration of Wigner–Seitz radii R_{ws} and by the topological atom method of Bader.[20,21] Rather than dividing space into hard spheres (R_{ws}), the approach of Bader is to divide space into atomic regions determined by zero-flux charge-density surfaces.[20] The difference between the number of valence electrons contained within a volume and the number assigned to the neutral atom is defined here as the oxidation state. The values of R_{ws} were initially set to the crystal radii[22] and were increased to allow the total volume of the cell to be filled. The final radii used were 2.15 Å for Cs, 1.3 Å for Cu, 1.45 Å for Ag, 1.35 Å for U, and 2.0 Å for S.

Previous local density approximation (LDA) calculations that used the linearized augmented plane-wave (LAPW) method in the AYMSe$_3$[3] and ALnMTe$_3$[5] systems have demonstrated some reliability in the determination of band gaps, despite the fact that LDA band structures frequently underestimate band gaps. The open-core schemes used in that previous work to handle the 4f electrons cannot be used here because of the lesser degree of 5f electron localization. To our knowledge the incorporation of the Hubbard U parameter in the LDA+U or local spin-density (LSDA+U) approximations has not been successfully applied to actinide compounds beyond the binary oxides,[23,24] binary chalcogenides,[25] and ternary intermetallics.[26,27] Even when a full-potential fully relativistic LSDA+U method is applied in the intermetallic systems, experimental property values must be used to fit Coulomb and exchange parameters.[27] The addition of the Hubbard U parameter to the current calculations would serve to shift the Fermi energies and possibly the band gaps, but we believe it would yield little additional information about the electronic structures. Similarly, spin−orbit effects are possibly important, as they significantly impact the distribution of occupied states for heavy elements. Some exploratory calculations including the spin−orbit interaction were made in the PAW-GGA pseudopotential context. Our preliminary conclusion is that such effects are primarily of importance in determining the spatial orientation of the uranium magnetic moments, a subject we will treat elsewhere because multiple crystallographic unit cells are required to map out distinct magnetic unit cells.

Experimental Results

Syntheses. The synthesis conditions of the title compounds differed from those used in the syntheses of the previously reported CsCuUSe$_3$, [1] CsCuUTe$_3$,[9] or KCuUSe$_3$[8] compounds. The Q/A$_2$Q ratio was larger; this less basic reaction condition is important for the crystallization of the sulfides and the Ag analogues. Efforts to make Ag-containing tellurides were not successful.

Structures. The isostructural compounds KCuUS$_3$, RbCuUS$_3$, RbAgUS$_3$, CsCuUS$_3$, CsAgUS$_3$, RbAgUSe$_3$, and CsAgUSe$_3$ crystallize in the KCuZrS$_3$ structure type. The shortest S···S distance in any of the five sulfides is 3.693(1) Å in RbCuUS$_3$, and the shortest Se···Se distance in the two selenides is 3.899(1) Å. Because there are no Q−Q bonds in the structures, the oxidation states of 1+, 1+, 4+, and 2− may be assigned to A, M, U, and Q, respectively.

The structure is layered, as shown in a perspective view down [100] (Figure 1). Figure 2 shows an isolated $^2_\infty$[MUQ$_3^-$] layer, as viewed down [010]. The layers are separated by A atoms in bicapped trigonal-prismatic coordination. The layers of AMUQ$_3$ contain MQ$_4$ tetrahedra and UQ$_6$ octahedra. The MQ$_4$ tetrahedra share edges with the four adjacent UQ$_6$ octahedra; the UQ$_6$ octahedra are interconnected by edge-sharing two equatorial Q(1) atoms in the [100] direction and corner-sharing through the axial Q(2) atom in the [100] direction. Although all seven compounds

(14) Kresse, G.; Hafner, J. *Phys. Rev. B* **1993**, *47*, 558–561.
(15) Kresse, G.; Hafner, J. *Phys. Rev. B* **1994**, *49*, 14251–14271.
(16) Kresse, G.; Furthmüller, J. *Comput. Mater. Sci.* **1996**, *6*, 15–50.
(17) Kresse, G.; Furthmüller, J. *Phys. Rev. B* **1996**, *54*, 11169–11186.
(18) Kresse, G.; Joubert, D. *Phys. Rev. B* **1999**, *59*, 1758–1775.
(19) Monkhorst, H. J.; Pack, J. D. *Phys. Rev. B* **1976**, *13*, 5188–5192.
(20) Henkelman, G.; Arnaldsson, A.; Jónsson, H. *Comput. Mater. Sci.* **2006**, *36*, 354–360.
(21) Sanville, E.; Kenny, S. D.; Smith, R.; Henkelman, G. *J. Comput. Chem.* **2007**, *28*, 899–908.
(22) Shannon, R. D. *Acta Crystallogr., Sect. A* **1976**, *32*, 751–767.
(23) Geng, H. Y.; Chen, Y.; Kaneta, Y.; Kinoshita, M. *Phys. Rev. B* 2007, *75*, 054111−1-8.
(24) Maehira, T.; Hotta, T. *J. Magn. Magn. Mater.* **2007**, *310*, 754–756.
(25) Antonov, V. N.; Harmon, B. N.; Yaresko, A. N.; Perlov, A. Y. *Phys. Rev. B* **1999**, *59* (22), 14571–14582.
(26) Rusz, J.; Divis, M. *J. Phys.: Condens. Matter* **2004**, *16*, 6675–6684.
(27) Rusz, J.; Divis, M. *J. Magn. Magn. Mater.* **2005**, *290−291*, 367–370.

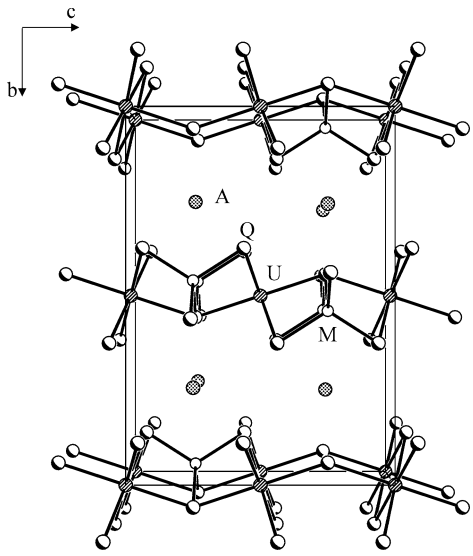

Figure 1. Unit cell of the $AMUQ_3$ structure viewed down [010].

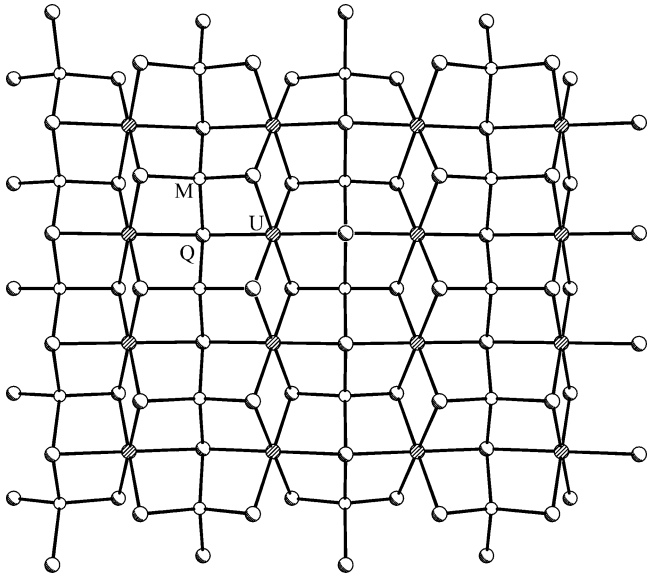

Figure 2. The $^{2}_{\infty}[MUQ_3^-]$ layer in the $AMUQ_3$ structure.

are isostructural, the CuQ_4 tetrahedra and the UQ_6 octahedra in the three Cu-containing compounds are only slightly distorted, whereas the AgQ_4 tetrahedra and consequently the UQ_6 octahedra in the four Ag-containing compounds are more distorted. For example, the Q−Cu−Q angles range from 106.95(2) to 117.20(8)°, whereas the Q−Ag−Q angles range from 105.45(5) to 126.79(9)° (Table 2).

Selected interatomic distances for these seven compounds are listed in Table 2. These distances are normal. The ranges of distances are Cu−S, 2.321(2)−2.413(1) Å; Ag−S, 2.490(2)−2.552(2) Å; Ag−Se, 2.593(9)−2.6470(9) Å; U−S, 2.7064(7)−2.759(1) Å; U−Se, 2.8693(6)−2.8750(5) Å; K−S, 3.190(3)−3.585(2) Å; Rb−S, 3.310(2)−3.626(2) Å; Cs−S, 3.471(2)−3.706(2) Å; Rb−Se, 3.416(1)−3.6166(9) Å; and Cs−Se, 3.576(1)−3.7453(7) Å. These ranges are consistent, for example, with those of 2.3530(9)−2.4025(8) Å for Cu−S in KNd_2CuS_4,[28] 2.502(1)−2.864(1) Å for Ag−S in $CsAgSb_4S_7$;[29] 2.6135(8)−2.766(1) Å for Ag−Se in $CsTb_2Ag_3Se_5$;[30] 2.753(2)−2.825(2) Å for U−S in US_3; 2.839(1)−2.848(1) Å for U−Se in $KCuUSe_3$;[8] 3.164(1)−3.7841(5) Å for K−S in KNd_2CuS_4;[28] 3.293(1)−3.460(1) Å for Rb−S in $RbGd_2CuS_4$;[31] 3.486(2)−3.608(1) Å for Cs−S in $CsYbZnS_3$;[4] 3.4299(8)−3.7833(6) Å for Rb−Se in $RbYbZnSe_3$;[4] and 3.5993(8)−3.9101(7) Å for Cs−Se in $CsGdZnSe_3$.[1]

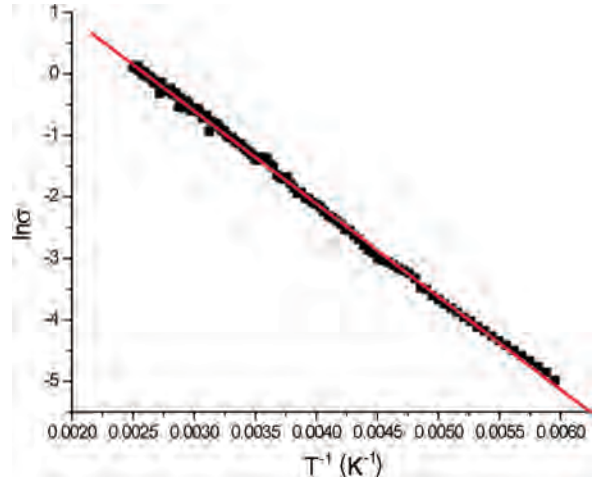

Figure 3. ln σ vs $1/T$ for $CsCuUS_3$.

Optical Properties. The nature of the optical band gaps observed in these layered materials that possess the $KCuZrS_3$ structure type has been discussed previously.[3,5] Electronic band-structure calculations of isostructural $AMLnQ_3$ rare-earth materials indicate that they are direct band-gap semiconductors whose optical band gaps can be tuned by crystal orientation as well as by chemical substitution of Ln, M, and Q.[3,5] Moreover, it was found that the alkali metal A does not contribute to the DOS near the Fermi level. This confirmed the experimental observations that the physical properties of these materials are not affected by alkali-metal substitution.[4] The main conclusions from the earlier theoretical studies are that the $[MLnQ_3^-]$ layer and its relative covalency ultimately govern the optical properties of these materials.

Note that the optical properties of only two actinide compounds possessing the $KZrCuS_3$ structure type, namely $KCuUSe_3$[8] and $KCuThS_3$,[32] have been measured to date. As occurs in the $AMLnQ_3$ materials, chalcogen substitution in the $KCuThQ_3$ materials alters the optical band gaps. Thus, these f^0 Th(IV) materials show different colors: $KCuThS_3$ is colorless,[32] whereas $KCuThSe_3$ is red.[33]

Single-crystal optical measurements on the present $AMUS_3$ (A = Rb, Cs; M = Cu, Ag) materials indicated total absorbance from 900 to 1700 nm. Hence, all of these $AMUS_3$ compounds have band gaps smaller than 0.73 eV, whereas the isostructural $KCuThS_3$ compound has a band gap of 2.95 eV.[32] Thus, it is clear that the more diffuse 5f electrons play a dominant role in the optical properties of these materials. For the rare-earth analogues, the number of 4f electrons does not have such an influence on the optical band gaps. Similar to all materials possessing the $KCuZrS_3$ structure type, the physical properties of the $AMUS_3$ compounds should also be tunable by means of M or Q substitution.

Electronic Conductivity. Figure 3 displays the dependence of the electrical conductivity of $CsCuUS_3$ on temperature. The conductivity along [100] is 0.3 S/cm at 300 K. Below 168 K, the sample resistance increased beyond the detection limits of the instrument. The material is seen to be a semiconductor with a simple Arrhenius-

(28) Yao, J.; Deng, B.; Ellis, D. E.; Ibers, J. A. *J. Solid State Chem.* **2003**, *176*, 5–12.
(29) Huang, F. Q.; Ibers, J. A. *J. Solid State Chem.* **2005**, *178*, 212–217.
(30) Huang, F. Q.; Ibers, J. A. *J. Solid State Chem.* **2001**, *158*, 299–306.
(31) Yao, J.; Ibers, J. A. *Acta Crystallogr., Sect. E* **2004**, *60*, i95–i96.
(32) Selby, H. D.; Chan, B. C.; Hess, R. F.; Abney, K. D.; Dorhout, P. K. *Inorg. Chem.* **2005**, *44*, 6463–6469.
(33) Narducci, A. A.; Ibers, J. A. *Inorg. Chem.* **2000**, *39*, 688–691.

Table 3. Oxidation-States (e^-)[a]

	Wigner–Seitz radii method		Bader method	
atom	Cu	Ag	Cu	Ag
Cs	0.98	1.00	0.79	0.80
M	0.91	1.00	0.44	0.25
U	3.98	4.01	1.91	1.92
S1	−2.20	−2.04	−1.03	−0.96
S2	−1.90	−1.83	−1.06	−1.00

[a] Difference between the number of valence electrons contained within a volume and the number assigned to the neutral atom.

type thermal activation $\sigma = \sigma_o \exp-(E_a/(k_B T))$, with an activation energy E_a of 0.14 eV. For intrinsic semiconductors, $E_a \approx 1/2\ E_{gap}$.[34] Thus, the band gap should be approximately 0.3 eV, consistent with the result of the optical measurement. Although this band gap is close to the optimum one[35] of 0.25 eV for thermoelectric applications at 298 K, the conductivity of $CsCuUS_3$ is too low.

Theoretical Results

Relaxed Structure and Charge Distributions. Structural relaxation of ions contained within the fixed 153 K unit cells of $CsCuUS_3$ and $CsAgUS_3$ resulted in less than 0.009Å movement in any one direction; this is close to the accuracy of the unit cell constants.

Oxidation state analyses within spherical volume integration (R_{ws}) and Bader topological atom methodologies showed very different atomic charges (Table 3). With a reasonable choice of radii, the R_{ws} method yielded the expected oxidation states for all atoms, but this is of course subject to careful interpretation. The charge difference between atoms S1 and S2 can be attributed to differing U−S and M−S interatomic distances (Table 2); shorter interatomic distances lead to greater U−S or M−S overlap. This difference is less apparent in the Bader method, perhaps because the volume attributed to each S atom by the zero-flux charge surface depends most significantly upon the atomic coordination. We might expect that Bader analysis would decrease the ambiguity in the interpretation of oxidation states, but at first glance it seems to yield little chemically relevant information. The anions and cations are correctly identified, but with the exception of Cs, the charge on each is approximately half of that expected on the basis of formal charge. This decrease in charge in part can be attributed to the degree of covalent bonding in the $^2_\infty[UMS_3^-]$ layers. Part a of Figure 4 displays a two-dimensional charge density map parallel to the (010) plane, that of the $^2_\infty[UMS_3^-]$ layer. The bond lines among U, S, and Cu are not fully contained within this plane, but the degree of overlap among U, S, and Cu electron clouds is clearly evident from this cross section. Part b of Figure 4 displays a cross section parallel to the (001) plane where one can see both the lack of overlap between Cs and the $^2_\infty[UMS_3^-]$ layers and again the overlap within the layer. The Cs is clearly ionic whereas there is covalent bonding within the $^2_\infty[UMS_3^-]$ layers.

Partial Densities of States. Figure 5 shows the partial (PDOS) and total densities of states (DOS) of $CsCuUS_3$ and $CsAgUS_3$. As is common to DFT calculations, the model fails to place accurately the Fermi energy in the band gap; a naive interpretation is that both materials are metallic. Examination of the PDOS shows that the U 5f orbital is responsible for most of the character of the low-lying conduction band; U−S covalency effects also pull a small amount of S excited states below E_f. The calculated band gaps (Cu 1.34 and Ag 1.51 eV) overestimate by almost a factor of 2 those deduced from the optical data; this is surprising in view of typical LSDA underestimates. It is tempting to assign the conductivity gap to impurity levels. However, elemental analysis and the simple temperature dependence of the conductivity indicate that the conductivity is intrinsic. Presumably, addition of the Hubbard U parameter (LSDA+U method) would serve primarily to open the U 5f occupied−unoccupied gap. This would transform the metallic structure into a semiconductor but would only worsen the comparison of gap between theory and experiment.

Let us examine the PDOS in more detail. As would be expected from the electron density maps, the Cs electrons in both compounds make little contribution around the Fermi energy with the 5s electron density isolated at −22 eV and 5p electrons isolated between −10 and −8.5 eV, consistent with previous calculations on Cs and K rare-earth transition-metal chalcogenides.[3,5,28] Previous experimental evidence shows the substitution of Cs for Rb in isostructural lanthanide compounds also produces little effect on the optical band gaps[4] and consequently the alkali-metal cation contributes little density near the Fermi level. The electronic properties will therefore be characteristic of the $^2_\infty[UMS_3^-]$ layers and similar throughout the five sulfide compounds synthesized. As indicated in Figure 5, the occupied-state density forming the top of the valence bands is composed of M−S overlap regions: Cu/Ag−S is dominant, but some significant U−S contributions are seen as evidence of covalency. Thus, in $CsCuUS_3$, part a of Figure 5, the valence band below the Fermi energy between −6.5 and −1.2 eV consists of extensive overlap of Cu 3d electrons and S 3p electrons with a small contribution from the U 5f electrons. In $CsAgUS_3$ (part b of Figure 5), the overlap region is markedly different; there is considerable overlap at approximately −5.5 eV, but only small M contributions between −5 and −1.3 eV. In both compounds, this M−S overlap region is in direct contrast to that seen in previous DOS calculations on the isostructural $CsYMSe_3$ (M = Zn, Cd, Hg)[3] and $CsTbZnTe_3$[5] compounds. In those compounds, the majority of density in the valence bands consists of chalcogenide p electrons, whereas the majority of the metal-center density is located in the conduction bands. The present valence-band overlap is similar to that seen in the DOS of KSm_2CuS_4, where overlap of the Cu 3d and S 3p electron forms the valence band and the Sm 4f electrons form the conduction band.[28] The splitting of the S 3p electron density into both valence and conduction bands is unique to the present actinide compounds and is clearly the result of covalent interactions with U 5f electrons. In both $CsCuUS_3$ and $CsAgUS_3$, the conduction band is predominately composed of U 5f and S 3p overlap with small contributions from M. The DOS also

(34) Kittel, C. *Introduction to Solid State Physics, 7th ed.*; Wiley: New York, 1996.
(35) Sofo, J. O.; Mahan, G. D. *Phys. Rev. B* **1994**, *49*, 4565–4570.

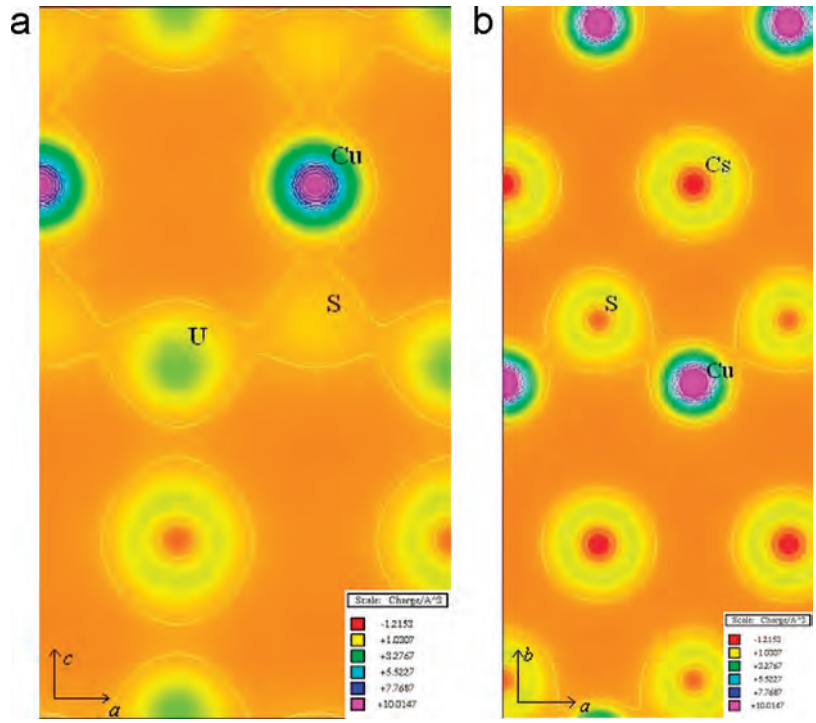

Figure 4. Two-dimensional electron density maps: (a) cross section parallel to (010) containing U, Cu, and S atoms, (b) cross section parallel to (001) containing Cs, Cu, and S atoms. Equal-interval contours are shown.

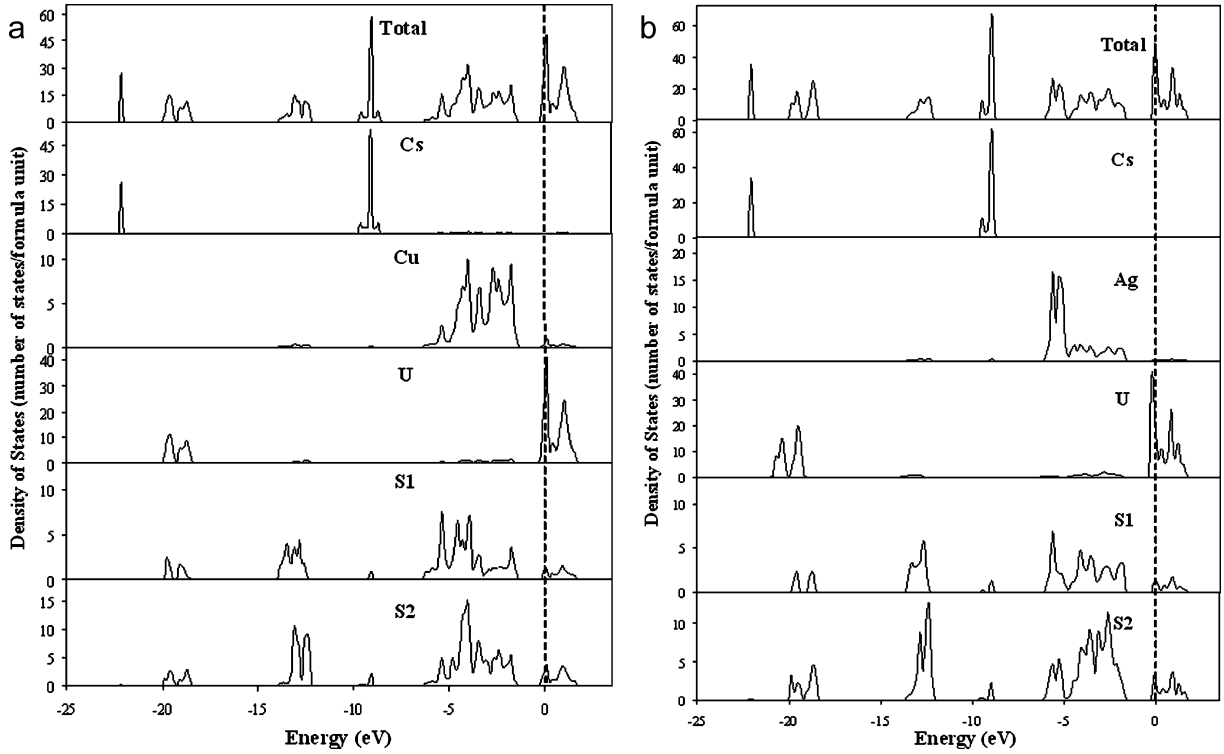

Figure 5. Partial (PDOS) and total density of states (DOS) for (a) $CsCuUS_3$ and (b) $CsAgUS_3$.

shows an increase in the band gap from 1.34 eV for $CsCuUS_3$ to 1.51 eV for $CsAgUS_3$. This increase in band gap as one descends a group in the periodic table is also seen in going from Zn to Cd to Hg in analogous rare-earth $ALnMQ_3$ compounds of the same structure type[3]

Spin Moments and Magnetic Order. Initial spin relaxation of an isolated Cu or Ag magnetic moment resulted in all the spin density moving to the U atoms. This is expected for monovalent s^0d^{10} Cu(I) and Ag(I). In the initial spin relaxation of an isolated U magnetic moment, the U atoms relaxed to two different antiferromagnetic (AF) spin states depending upon the coinage metal. In $CsCuUS_3$, the U atoms within $^2_\infty[UMQ_3^-]$ layers aligned antiparallel, whereas those closest between layers aligned parallel (AFI). In $CsAgUS_3$, U atoms within $^2_\infty[UMQ_3^-]$ layers aligned parallel and between $^2_\infty[UMQ_3^-]$ layers aligned antiparallel (AFII). An-

Table 4. Spin Relaxations (μ_B/U) of U Magnetic Moments and Total Energies (eV)

	$CsCuUS_3$		$CsAgUS_3$	
	AFII[b]	AFIII	AFII	AFIII
U1[a]	1.83	−1.86	1.91	−1.89
U2	1.91	1.86	1.89	1.89
U3	−1.91	1.86	−1.92	1.89
U4	−1.83	−1.86	−1.90	−1.89
energy[c]	0.00	0.25	0.00	0.22

[a] U1 is located at 0,0,0; U2 at 0,0,$^1/_2$; U3 at $^1/_2$,$^1/_2$,0; U4 at $^1/_2$,$^1/_2$,$^1/_2$. [b] AFII: U within $^2_\infty$[UMQ_3^-] layer parallel, between layers antiparallel; AFIII: all antiparallel. [c] Relative to the lowest-energy configuration.

other possible arrangement (AFIII) would be U atoms aligned antiparallel within and between $^2_\infty$[UMQ_3^-] layers. The final relaxed total spin magnetic moments converged to 1.9 μ_B/U in all three cases and only differed by alignment and total energy (Table 4). From calculations with *k*-point meshes of 9 × 9 × 9 it was found that for each of the Cu and Ag compounds the AFII magnetic structure was lowest in energy, the AFIII alignment was a local minimum, but the AFI magnetic structure was not stable. The two alignments where U atoms contained within $^2_\infty$[UMQ_3^-] layers were antiparallel (AFI and AFIII) were approximately 0.2 eV higher in energy. Interestingly, $CsYbZnSe_3$ displays a broad magnetic transition at ∼10 K.[2,3] A recent calculation[36] determined that the AFII alignment of Yb^{3+} ions in this structure was also lowest in energy. The predicted antiferromagnetic behavior in $CsCuUS_3$ and $CsAgUS_3$ is consistent with the observation of negative Weiss constants in a number of $ALnMQ_3$ compounds[2–4,6] and $KCuUSe_3$.[8] Other low-lying magnetic structures are certainly possible. The present model constrains the magnetic unit cell to the crystallographic unit cell with four U per unit cell. The closest U−U pairs within this unit cell are U1−U1 and U2−U2, which are separated by the length of the *a* axis, approximately 4.0 Å; this places a strong constraint on in-plane alignment. More extensive calculations that investigate the size of the magnetic unit cell are required.

Acknowledgment. This research was supported by the U.S. Department of Energy BES Grant ER-15522. Use was made of the Central Facilities supported by the MRSEC program of the National Science Foundation (DMR05-20513) at the Materials Research Center of Northwestern University. We thank Dr. Kenneth G. Spears for the use of his NIR spectrometer.

Supporting Information Available: Crystallographic files in CIF format for $KCuUS_3$, $RbCuUS_3$, $RbAgUS_3$, $CsCuUS_3$, $CsAgUS_3$, $RbAgUSe_3$, and $CsAgUSe_3$. This material is available free of charge via the Internet at http://pubs.acs.org.

IC800424T

(36) Chan, G. H.; Lee, C.; Dai, D.; Whangbo, M.-H.; Ibers, J. A. *Inorg. Chem.* **2008**, *47*, 1687–1692.